Hydrodynamics in a stirred tank with a retreat blade impeller: Evaluating the potential of IBM-LES through comparison with PIV data

Seyed Salar Hoseini, Ali Hamieh, Carole Coufort-Saudejaud, Christine Frances, Alain Liné, Jérôme Morchain

▶ To cite this version:

Seyed Salar Hoseini, Ali Hamieh, Carole Coufort-Saudejaud, Christine Frances, Alain Liné, et al.. Hydrodynamics in a stirred tank with a retreat blade impeller: Evaluating the potential of IBM-LES through comparison with PIV data. Chemical Engineering Research and Design, 2025, 215, pp.419-429. ⟨10.1016/j.cherd.2025.02.009⟩. ⟨hal-05036865⟩

HAL Id: hal-05036865
https://hal.inrae.fr/hal-05036865v1

Submitted on 3 Dec 2025

Title : **Hydrodynamics ina stirred tank with a Retreat Blade Impeller: evaluating the potential of IBM-LES through comparison with PIV data**

Authors : S.S. Hoseini, A. Hamieh, C. Coufort-Saudejaud, C. Frances, A. Line, J. Morchain:,

Article published in Chemical Engineering Research and Design

ChERD, 215, 419-429, 2025
https://doi.org/10.1016/j.cherd.2025.02.009

Received 28 November 2024, Revised 23 January 2025, Accepted 8 February 2025, Available online 10 February 2025, Version of Record 14 February 2025.

Hydrodynamics in a stirred tank with a Retreat Blade Impeller: evaluating the potential of IBM-LES through comparison with PIV data

Seyed Salar Hoseini[1], Ali Hamieh[1,2], Carole Coufort-Saudejaud[2], Christine Frances[2], Alain Line[1], Jérôme Morchain[1*]

(1) Toulouse Biotechnology Institute, Université de Toulouse, CNRS, INRAE, INSA, Toulouse, France

(2) Laboratoire de Génie Chimique, Université de Toulouse, CNRS, INPT, UPS, Toulouse, France

*Corresponding author: jerome.morchain@insa-toulouse.fr (J. Morchain)

Abstract: This work presents numerical and experimental studies on the turbulent flow in a stirred tank reactor equipped with a two-finger baffle and a retreat blade impeller at Re = 43,200. Numerical results were obtained from Large Eddy Simulation (LES) combined with an Immersed Boundary Method (IBM) for the impeller and baffle representation. The experimental data consists in a set of PIV measurements in a vertical plane containing the shaft axis. The numerical results are compared with experimental data in terms of the flow field, mean velocity components, and kinetic energy. Proper Orthogonal Decomposition (POD) is applied to the IBM-LES results to extract the dominant modes and their time coefficients. The POD analysis suggests that the high energy level found in the upper part of the tank results from an energy transfer from the coherent structures created downstream the two-finger baffle. Finally, the trailing vortices behind the impeller blades and the baffle were detected and visualized using Jeong and Hussain's technique. The results show that IBM-LES is a reliable tool for studying the unsteady characteristics of turbulent flow in agitated tanks with complex geometry.

Keywords: Retreat-blade impeller, immersed boundary method, computational fluid mechanics, turbulence, large eddy simulation.

1. Introduction

Stirred tanks are routinely used in many industrial applications such as pharmaceutical, biotechnology, food and beverage industries, water treatment, mineral processing, paint and coating production, etc. [1-3]. In most cases the flow structure is complex and difficult to figure out, hence the development of experimental and numerical techniques was dedicated to that purpose. Within the class of optical methods, Particle Image Velocimetry (PIV) has now become a standard [4, 5]. It is highly accurate but limited to laboratory scale, transparent devices, and transparent fluids. Computational Fluid Dynamics (CFD) modeling is a simulation technique providing cost-effective and accurate information about flow behaviors in stirred tanks [6, 7]. It is routinely used to design, optimize [8], and scale up [9] stirred tanks. Thanks to computational simulation techniques one can access comprehensive information on real-world and large-scale mixers. The challenges ahead for the numerical study of turbulent flow in stirred tanks include the choice of an appropriate turbulence model if an Unsteady Reynolds Average Navier-Stokes (U-RANS) approach is selected and the description of the impeller motion. As far as turbulence modeling is concerned, the Large Eddy Simulation (LES) technique is advantageous since there is no assumption on the turbulence structure but it comes with a higher computational cost due to fine meshing and high temporal resolution. Besides turbulence modeling, various strategies can be used to account for the impeller motion. The most popular are the Moving Reference Frame (MRF) [10, 11], the Sliding Mesh (SM) technique which emerged in the early 90’s [12, 13] and the Immersed Boundary Method (IBM) originally developed by Peskin [14].

The MRF is known to be the easiest to set-up, simply requiring separating the mesh into two zones: one related to the impeller (inner zone) and another for the rest of the fluid domain (outer zone). Momentum sources are added in the inner zone to model the impeller motion. It is recommended for unbaffled stirred tanks [15, 16]. However, this method is limited to steady-state simulation and only considers a particular position of the impeller relative to the baffles, if present. The Sliding Mesh technique basically consists in rotating the inner mesh zone and sliding it along the interface between the inner and outer zones, hence the name of the technique. It implies running transient simulations. The use of the SM technique is computationally demanding, and attention must be paid to mesh quality, mesh movement algorithms, and solver settings to ensure accurate and stable simulations. The Immersed Boundary Method conceptually differs from the previous ones in the sense that the impeller is not physically present in the computational domain but represented as a time-varying source term in the momentum equations. In terms of meshing, the main advantage of IBM is a simplified mesh generation process for complex geometries (e.g., complex impeller shape). Moreover, the conservative non-dissipative structured solver used in IBM is adapted to eddy-resolving methods such as LES [17]. Today, IBM-based algorithms are used in a wide variety of flow systems with complex and irregular geometries including, but not limited to, biological flow [18], mixed flow pumps [17], flow around an arbitrarily moving body [19], simulation of particulate flows [20, 21], etc.. In 2004, Verzicco *et. al* [22]., for the first time, used the IBM to perform LES and Direct Numerical Simulations (DNS) of the flow in a cylindrical un-baffled stirred tank equipped with a radial impeller at mid-height of the tank, at a Reynolds number of 1636, i.e. in the transition regime. The LES results were in good agreement with the available experimental data in terms of mean velocity profile. The authors also concluded that the LES with dynamic sub-grid model can provide the same results as DNS, whilst being more cost-effective numerically. Other examples using IBM in stirred tanks can be found in [23, 24]. A combination of LES and IBM was used to evaluate the role of impeller speed perturbation on the scalar mixing in a stirred tank [25], to simulate flow patterns in un-baffled and baffled stirred tanks equipped with pitched blade impeller [26] or to study the flow in a stirred tank equipped with a pitched blade impeller developing a parallel and adaptive algorithm [27].

The present study focuses on a stirred tank equipped with a retreat-blade impeller and a two-finger baffle. Retreat-blade impellers have been used in the fine chemical, pharmaceutical, and biopharmaceutical industries for over 30 years. However, the number of studies dedicated to them is rather limited. Campolo et al. [9, 28] conducted pioneering studies to numerically predict macro mixing performances, including power consumption and pumping efficiency in two different industrial-scale reactors equipped with retreat-curve impellers. One limitation of this work is that it does not evaluate the turbulence behavior in this type of stirred tank. Following this, in 2005, the hydrodynamic behaviors of three laboratory-scale vessels of 0.5, 2, and 20 liters were studied. These vessels were geometrically similar and equipped with retreat-curve impellers and cylindrical baffles. These vessels mimic reactors widely used in the pharmaceutical and fine chemical industries. CFD simulations were used, and the results were validated using Laser

Doppler Anemometry (LDA) measurements and empirical power consumption literature data [29]. In 2007, an experimental and numerical research study was conducted to evaluate the flow and mixing characteristics of a retreat-curve impeller in a conical-based vessel [30]. CFD simulations with a standard k-ε turbulence model were utilized to predict flow patterns and power numbers under various configurations (baffle arrangements and impeller spacings). Flow visualization revealed that the region inside the conical base is effectively unbaffled, with strong tangential velocity components, but little axial or radial circulation. Recently, in 2017, Sirasitthichoke and Armenante investigated the power dissipation and power number correlation in a torispherical-bottomed vessel equipped with a retreat blade impeller under different baffling conditions [31]. They established correlations for the Power number over a wide range of Reynolds numbers ($1 < Re < 400,000$), and for several types of baffles (beavertail, D-type, H-type, finger-type, fin-type baffles). Interestingly, the authors, in another research study [32], compared various CFD simulation techniques (MRF, SM and Lattice Boltzmann Method) in terms of total energy dissipation and torque, but no comparison of experimental and simulated velocity profiles were reported.

The impact of different baffle types makes it difficult to understand flow dynamics in stirred tanks with retreat-blade impellers. Although CFD simulations and some experimental studies (like using LDA) have been used to investigate the hydrodynamics in these tanks, validating these models with experimental data, such as PIV, is still a challenge. This includes predicting local flow patterns and hydrodynamics. The aim of the current work is to perform the analysis of the flow structure in a stirred tank with a retreat blade impeller using a combination of numerical simulation (IBM-LES) and experimental PIV data. Beside the good agreement in terms of velocity profiles, it is found that the turbulent kinetic energy content increases with the distance from the impeller. This unexpected result motivated the use of POD for a better understanding of the contribution of the baffle to flow unsteadiness. IBM-LES results collected in the PIV data plane were processed to extract the dominant modes and their time coefficients. A POD analysis of IMB-LES data in the impeller swept zone is an originality of this work and proved to be rather straightforward owing to the absence of mesh motion. It alleviates the cumbersome procedure previously developed by Mayorga et al. to perform flow analysis and reconstruction based on Sliding Mesh simulation data [33].

2. Stirred tank configuration

A sketch of the stirred tank and impeller geometries considered in this study is shown in Fig. 1**.** The total volume of the tank is 20 Liters with a working volume of 8 Liters. A three-blade impeller named Retreat Blade Impeller (Fig. 1b), is used to mix the fluid in the tank. Its diameter is 161 mm. It is mounted on a 10 mm shaft and placed in the center of the stirred tank, at 25 mm from the bottom. A high-performance Ika EUROSTAR 400 digital motor is used to drive the shaft. The rotational speed of the impeller is set at 100 RPM. To limit the formation of a central vortex in the tank and the deformation of the free surface, a baffle with two fingers oriented towards the center of the tank is positioned 65 mm from the bottom and 20 mm from the wall (Fig. 1c). Exact dimensions of the different elements are presented in Fig. 1e.

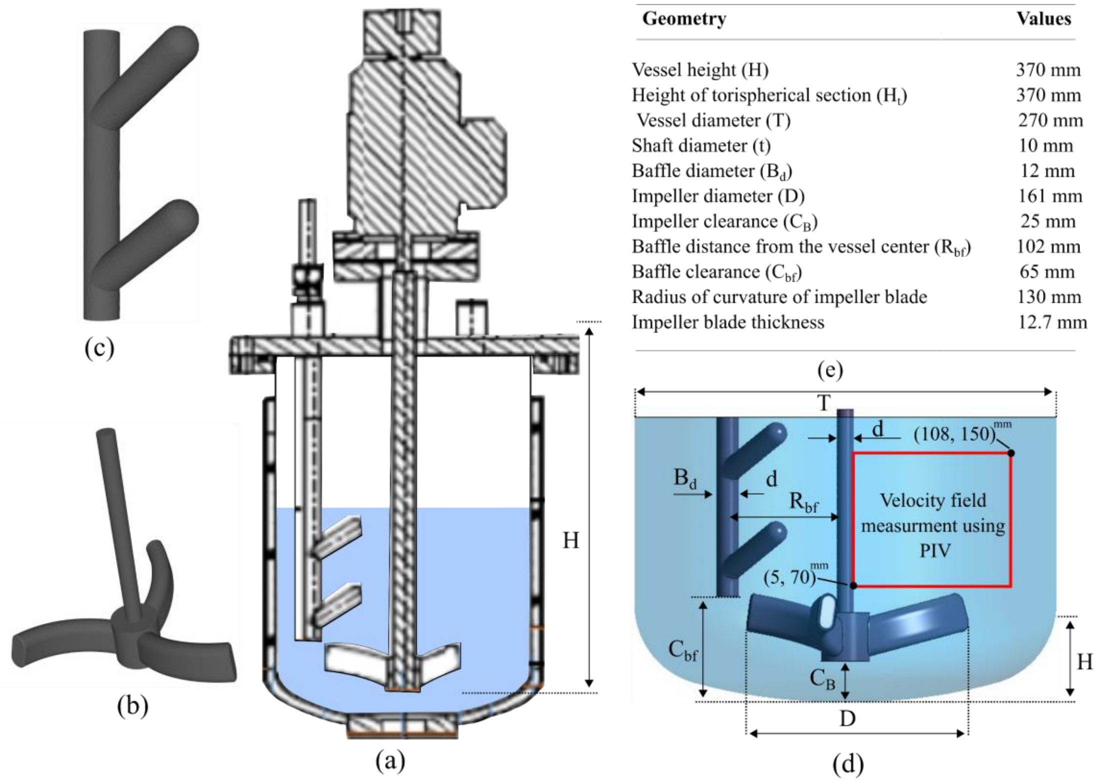

Geometry	Values
Vessel height (H)	370 mm
Height of torispherical section (H_t)	370 mm
Vessel diameter (T)	270 mm
Shaft diameter (t)	10 mm
Baffle diameter (B_d)	12 mm
Impeller diameter (D)	161 mm
Impeller clearance (C_B)	25 mm
Baffle distance from the vessel center (R_{bf})	102 mm
Baffle clearance (C_{bf})	65 mm
Radius of curvature of impeller blade	130 mm
Impeller blade thickness	12.7 mm

Fig. 1 : (a) Sketch of the experimental device; (b) retreat blade impeller; (c) two-finger baffle; (d) Details of the simulated geometry (the PIV window is marked in red); (e) dimensions of the different elements.

Considering the rotation speed of the impeller, the properties of water and an impeller Power number of 0.529, the Reynolds number is 43,200 and the flow regime is fully turbulent.

The power number was estimated using the correlation established by Sirasitthichoke and Armenante in a similar configuration [31]. The estimated volumetric dissipation rate in the stirred tank $\langle \varepsilon \rangle$ is about 0.03 m^2/s^3.

2.2. PIV experiments:

In-plane 2D 2C PIV measurements were carried out in a vertical plane described in Fig. 1**d**. In the following, *z* refers to the vertical coordinate, along the rotation axis, and *x* refers to the radial coordinate. In-plane 2D 2C means that only two components of the velocity vector are retrieved from the images, the orthoradial component is not measured. Images are acquired in a vertical plane containing the symmetry axis of the tank, located 120° downstream the baffle (in the direction of the flow). The 108 mm × 108 mm window is vertically centered around the horizontal line $\frac{z}{T} = \frac{1}{3}$ and spans the range $0.018 < \frac{x}{T} < 0.26$. The PIV system includes a double-cavity Nd: YAG laser which generates light pulses of 45 mJ at a wavelength of 532 nm and a Nikon Micro-Nikkor 105 mm f/2.8G camera (3 kHz at a resolution of 2032 × 2032 pixel). The camera is equipped with an appropriate filter centered on the emission wavelength of the seeding particles (532 nm) to obtain the best signal quality and to avoid spurious reflections from ambient lighting. Spherical fluorescent polymer particles (PMMA-RhB) with the range size of 1 - 20µm were used as seeding particles. The velocity field is analyzed with adaptive cross-correlation of 50% overlapping windows with interrogation cell sizes of 16×16 $pixels^2$. With these settings, the 16 pixels interrogation area corresponds to the special resolution Δz= 852 µm which also constitutes the PIV filter size. In addition, the filter should be smaller that Taylor microscale to correctly estimate TKE

For each set of PIV measurements, 5000 pairs of images were taken at 10 Hz which corresponds to a total survey time of 500 seconds. At N = 100 rpm, a blade passes through the measuring plane every 0.2 seconds. Consequently, during an acquisition time of 500 seconds, 2500 blade passages are recorded in the database. The statistical convergence of the ensemble and fluctuating velocities was checked in different locations (see supplementary information **Fig. S1-S4**).

3. Numerical Methodology

3.1. IBM-LES

The governing equations for LES are derived by applying a filtering operation to the time-dependent Navier-Stokes equations in physical space. The resulting governing equations for incompressible flows are as follows:

$$\nabla \cdot \hat{\boldsymbol{u}} = 0 \tag{1}$$

$$\frac{\partial \hat{\boldsymbol{u}}}{\partial t} + \nabla \cdot \hat{\boldsymbol{u}}\hat{\boldsymbol{u}} = -\nabla \hat{p} - \nabla \cdot \tau + \frac{1}{Re}\nabla^2 \hat{\boldsymbol{u}} + \mathbf{f} \tag{2}$$

In these equations, ^ represents filtered variables, t denotes time, Re is the Reynolds number, $\hat{\boldsymbol{u}}$ is the filtered velocity vector, $\hat{p}$ being a modified pressure that incorporates the trace of the SubGrid-Scale (SGS) viscous stress tensor τ and $\boldsymbol{f}$ representing a forcing term. The boundary body force $\boldsymbol{f}$ is prescribed at each time step to add momentum corresponding to the desired blade velocity onto an arbitrary surface that need not coincide with the grid. This method is known as the Immersed Boundary Method which basically models the solid surfaces as a source term in the fluid flow equations, forcing the fluid velocity to match the solid velocity. IBM was developed to deal with complex fluid-structure interaction situations in which the solid boundaries or submerged objects do not align with the computational grid [14]. Details on the implementation of this method can be found in [34].

In this study, the Smagorinsky-Lilly sub-grid closure model is employed to parameterize the SGS stresses [35]. The sub-grid model assumes that the Reynolds number is sufficiently high to ensure that energy is transferred from the large to the small scales, which are responsible for the energy dissipation [36]. It assumes a local equilibrium between production and dissipation of turbulent kinetic energy at the cut-off scale [37, 38]. The contribution of unresolved scales in the filtered Navier-Stokes equations are modeled using the eddy viscosity (3), where the eddy viscosity (v_t^{SM}) is defined by (4). [6, 17]. This sub-grid model is a popular and cost-effective choice in applications involving rotating machinery.

$$\tau - \mathrm{Tr}(\tau) = -2\nu_{\mathrm{t}}\widehat{\boldsymbol{S}} \tag{3}$$

$$\nu_t^{SM} = (C_s\Delta)^2|\widehat{\boldsymbol{S}}|, \text{ and } |\widehat{\boldsymbol{S}}| = (2\widehat{\boldsymbol{S}} \cdot \widehat{\boldsymbol{S}})^{1/2} \tag{4}$$

$\widehat{\boldsymbol{S}}$ represents the resolved strain rate tensor, C_s stands for the Smagorinsky constant, Δ is the local filter size, defined as the cubic root of the cell volume, and Tr(τ) is the sum of the normal stresses in the tensor τ. The Smagorinsky constant is set to 0.2 [6].

3.2. Meshing

The impeller swept zone is meshed using a fine structured mesh. The impeller blade surfaces are meshed using rectangular elements. The mesh grid near the tip of the blades is refined to get a more accurate description of actual shape in this zone. The immersed boundary is identified by three types of cells: (i) Fluid Cells having all their vertices located outside of the solid region; (ii) Immersed Boundary cells (they represent the interface between the fluid and the immersed boundary (solid structure) with vertices in both the fluid and solid regions; (iii) Solid Cells with their vertices in the solid region. Accordingly, the mesh has to be sufficiently fine to facilitate effective interpolation of fluid properties near the immersed-solid boundary. The meshing strategy is actually much simpler than when the Sliding Mesh technique is used, whilst the simulation does not entail computationally demanding mesh motion.

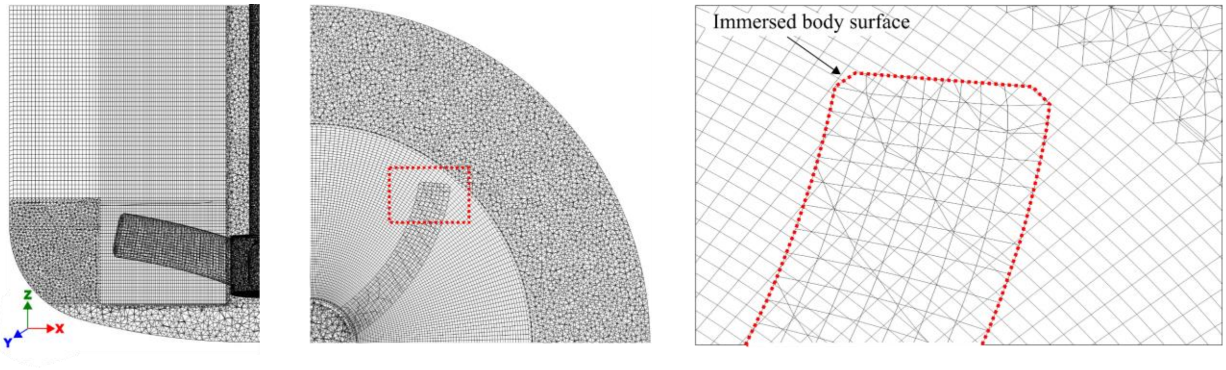

Fig. 2 : Mesh design employed for the IBM-LES simulations

A suitable mesh was obtained through a mesh independence study using experimental PIV data as a reference. A coarse mesh with 1,234,011 elements is compared to a finer mesh with 4,231,548 elements. The latter is presented in Fig. 2. As shown in Fig. 3, there are significant difference between the coarse mesh and the fine mesh in terms of ensemble average velocity prediction. The magnitude of the predicted velocity is in good agreement with the experimental results when the fine mesh is used. Also, this mesh will lead to a better resolution of the small scales of turbulence which can be inferred through the estimation of turbulent length scales presented in Table 1. In order to identify the suitable mesh size for LES simulations, a preliminary study using the SM-URANS approach and a standard turbulence model of k-ε was conducted (see details in the Supplementary Information).

Table 1: Comparison between the cell size and the turbulent length scales of the flow

	Mesh nmber (M)	Cell size (mm) [a]		Turbulent length scales (mm)	
		Min	Max	[b] $< \lambda >$	[c] $< \eta >$
Coarse	1.23	3	3.67	5.5	0.12
Fine	4.23	0.6	2.5		

[a] The cell size was calculated based on the cubic root of the cell volume

[b] Taylor micro scale $\lambda = (\frac{10\nu k}{\varepsilon})^{1/2}$ estimated from the computed turbulent kinetic energy k and resolved ε from SM-URANS simulation on the fine mesh (See Supplementary Information)

[c] Kolmogorov scale $\eta = \left(\frac{\nu^3}{\langle\varepsilon\rangle}\right)^{\frac{1}{4}}$ with $\langle\varepsilon\rangle$ estimated from the Power Number reported by Sirasitthichoke and Armenante, 2017 [31]

It is observed that the fine mesh has its maximum cell size two times smaller than the (smallest) Taylor micro-scale. Hence, it is expected to capture all scales of the turbulent kinetic energy with the fine mesh. In contrast, the min cell size is still ten times larger than the Kolmogorov length scale suggesting that the resolution is insufficient to capture all scales of energy dissipation rate, even with the fine mesh. Thus, the presented mesh is such that the LES simulation directly resolves all turbulent scales down to 10η, while the small-scale turbulence is filtered out. Indeed, Saarenrinne *et al.* showed that, for a stirred tank equipped with two-bladed paddle in turbulent regime and a specific resolution of 9η, only 65% of the dissipation rate was retrieved, while a resolution of 2η was required to achieve 90% [39].

The SM-URANS preliminary study revealed that the interaction of the rotating fluid motion and the baffle promotes the detachment of coherent structures in the wake of the baffle. The correct description of the energy transfer from these organized structure to the turbulent motion requests an appropriate choice of the turbulence model which is difficult to perform a priori. As it was beyond the scope of this study to compare the merits of the different turbulence models, efforts were put on the use of the IBM-LES approach, which makes fewer assumptions about turbulence structure.

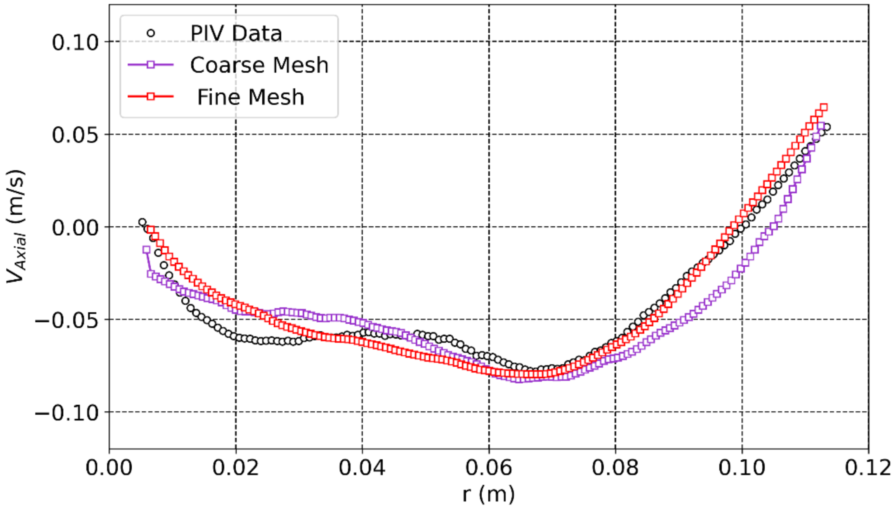

Fig. 3: Mesh sensitivity study for IBM-LES (Z = 0.085 m)

3.2. Computational aspects

All simulations were performed using CFX, ANSYS 2022 R2 using double-precision solver. The computational hardware includes a workstation equipped with Intel(R) Xeon(R) silver 4216 CPU @ 2.10GHz 2.10 GHz (2 processors) and NVIDIA Quadro P1000 graphics processor (GPU). Water at 25 °C, $\rho = 10^3\ kg.m^{-3}$, $\mu = 10^{-3}\text{Pa.s}$ was considered. The rotation speed, N, of the impeller is set to 100 RPM which results in a Reynolds number of 43,200 ($Re = \rho N D^2/\mu$) and a tip velocity of $0.84\ m.s^{-1}$. High-order schemes were employed for all equations, while the transient terms were discretized using the second-order backward Euler scheme. Convergence was judged based on normalized scaled residuals for continuity, momentum, and turbulence equations, with a convergence criterion set to10^{-6}. These criteria were met within a maximum of 10 iterations per time step. Unsteady simulations were run until robust statistical convergence on the mean and fluctuating velocities was achieved. The time step is set to 0.002 s which corresponds to an angular displacement of the impeller of 1.2°. During the simulations, results were stored every time step during 38 revolutions, which corresponds to approximately 23 seconds of real-time and 11,238 data files. Data recovery and processing are performed with an in-house python code.

The CFD results being time resolved (every 0.002 s or equivalently every 1.2°), one can produce phase-averaged results in 100 vertical planes (referred as k-plane) between two blades. The impeller having three blades, each impeller rotation produces three events for any k-plane, leading to a total of $n_a = 11{,}238/3 = 3776$ acquisitions for each angular position. In the following, each acquisition in a given k-plane is referenced by its index l.

3.3. Theory and data analysis

3.3.1. Triple decomposition of instantaneous IBM-LES velocities

In stirred tanks, especially in the impeller region, the local instantaneous velocity, $U_i^{k,l}(M,t)$ at each time step (k stands for a blade position and l stands for an event in that position) is usefully decomposed into an mean velocity, $\overline{U_i(M)}$, a periodic velocity, $\tilde{u}_i^k(M,t)$, and a fluctuating velocity $u_i'^{k,l}(M,t)$ [5, 6].

$$U_i^{k,l}(M,t) = \overline{U_i(M)} + \tilde{u}_i^k(M,t) + u_i'^{k,l}(M,t) \tag{5}$$

The mean components $\overline{U_i(M)}$ are determined by ensemble-averaging the 11,238 instantaneous velocity fields extracted from the simulation. It can also be regarded as the mean over all planes and all events by plane, thus leading to

$$\overline{U_i(M)} = \sum_{k=1}^{n_p} \frac{1}{n_p} \sum_{l=1}^{n_a} \frac{U_i^{k,l}(M,t)}{n_a} \tag{6}$$

Where, n_p is the blade positions between the passage of two blades. Introducing the phase-averaged

$$\left\langle U_i^k(M,t) \right\rangle = \sum_{l=1}^{n_a} \frac{U_i^{k,l}(M,t)}{n_a} \tag{7}$$

velocity

and considering that, by construction, the average of the fluctuating component $u_i'^{k,l}(M,t)$ over n_a independent events is zero, allows to express the periodic velocity as follows:

$$\tilde{u}_i^k(M,t) = \langle U_i^k(M,t)\rangle - \overline{U_i(M)} \tag{8}$$

Finally, injecting equation (8) in the definition (5) gives access to the fluctuating velocities

$$u_i'^{k,l}(M,t) = U_i^{k,l}(M,t) - \langle U_i^k(M,t)\rangle \tag{9}$$

3.3.2. Kinetic energy of IBM-LES

Following the velocity decomposition, three types of kinetic energy can be identified. The first kinetic energy is due to the mean flow, the second one is the periodic kinetic energy, k_p, related to the blade passage and the third one is the turbulent kinetic energy, k_t, related to turbulent fluctuations. The total kinetic energy, k_{tot}, is the sum of these three types of kinetic energy.

The periodic stress tensor can be calculated using equation (10) and the periodic kinetic energy k_p is readily deduced from it, according to equation (11).

$$\overline{\tilde{u}_i(M,t)\tilde{u}_j(M,t)} = \sum_{k=1}^{n_p} \frac{\tilde{u}_i^k(M,t)\tilde{u}_j^k(M,t)}{n_p} \tag{10}$$

$$k_p = \frac{1}{2}\sum_{i=1}^{3} \overline{\tilde{u}_i^2(M,t)} \tag{11}$$

The turbulent kinetic energy k_t is obtained in a similar way. The components of the turbulent stress tensor are obtained through an ensemble averaging which can also be regarded as double averaging as shown in equations (12) and (13) and the turbulent kinetic energy is calculated using (14).

$$\left\langle u_i'^{k}(M,t)u_j'^{k}(M,t)\right\rangle = \sum_{l=1}^{n_a} \frac{u_i'^{k,l}(M,t)u_j'^{k,l}(M,t)}{n_a} \tag{12}$$

$$\overline{u_i'^{k}(M,t)u_j'^{k}(M,t)} = \sum_{k=1}^{n_p} \frac{\left\langle u_i'^{k}(M,t)u_j'^{k}(M,t)\right\rangle}{n_p} \tag{13}$$

$$k_t = \frac{1}{2}\sum_{i=1}^{3} \overline{u_i'^{2}(M,t)} \tag{14}$$

3.3.3. Viscous dissipation of kinetic energy of IBM-LES

Theoretically, the turbulent kinetic dissipation rate (ε) can be estimated using (15) and involves the instantaneous velocity gradients at the Kolmogorov length scale [6].

$$\varepsilon = \nu\left(< S_{ij}S_{ij} >\right) = \frac{\nu}{2}\overline{\left(\frac{\partial u_i}{\partial x_j} + \frac{\partial u_j}{\partial x_i}\right)^2} \tag{15}$$

Since the mesh size is larger than the Kolmogorov length scale in LES simulations, only a part of the dissipation can actually be accessed from the resolved scales, $\hat{\boldsymbol{u}}$, and the other part is estimated using a so-called Sub-Grid Scale model (SGS).

Computation of sub-grid dissipation rate is given in equation (16)

$$\varepsilon_{\mathrm{SGS}} = \tau_{ij}S_{ij} = 2\nu_{\mathrm{T}}\hat{S}_{ij}\hat{S}_{ij} = \frac{\nu_{\mathrm{T}}}{2}\left(\frac{\partial \hat{u}_i}{\partial x_j} + \frac{\partial \hat{u}_j}{\partial x_i}\right)^2 \tag{16}$$

And the total energy dissipation rate can be computed from (17)

$$\varepsilon = 2(\nu_{\mathrm{T}} + \nu) < S_{ij}S_{ij} >= \frac{\nu_{\mathrm{T}} + \nu}{2}\left(\frac{\partial \hat{u}_i}{\partial x_j} + \frac{\partial \hat{u}_j}{\partial x_i}\right)^2 \tag{17}$$

4. Results and discussion

4.1. Mean flow field

The statistical convergence of the mean and RMS velocities is given as supplementary information (**Fig S1-S4**). Convergence is reached after 8000 acquisitions (a total of 11,238 being made).

Radial profiles for average velocity components of numerical results (IBM-LES) and PIV measurements for two axial positions Z =0.085 m and Z = 0.105 m are shown in Fig. 4. For the axial position Z =0.085 m, i.e., slightly above the impeller, IBM-LES gives a good estimation of axial mean velocity component. For the axial position Z = 0.105 m, i.e., far above the impeller, the agreement between the numerical results and the PIV data in terms of the axial mean velocity component is also acceptable. The main point for the Z = 0.105 m position is that the baffle plays an important role in flow structure. The results show that representing the baffle by an immersed solid boundary is a reasonable option.

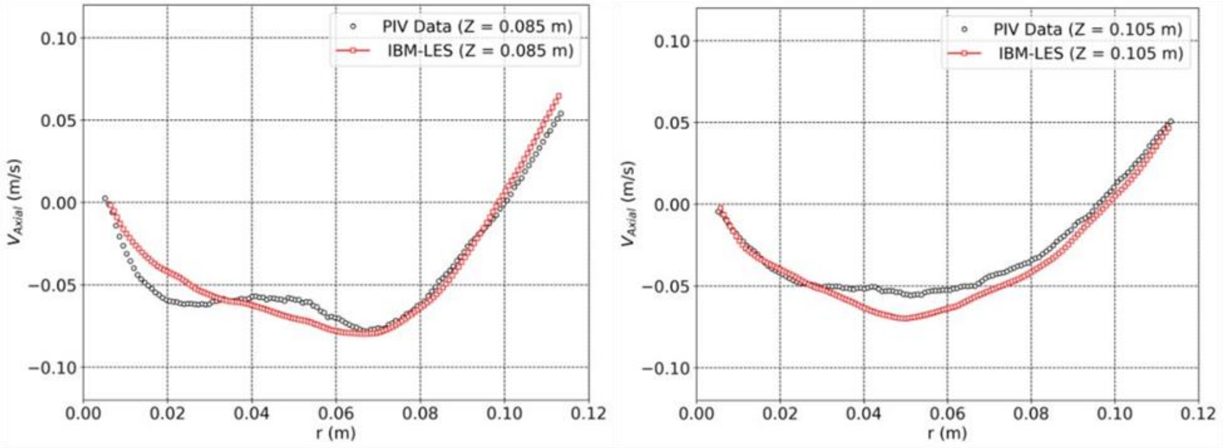

Fig. 4. Radial profile of the mean axial velocity at Z = 0.085 m and Z = 0.105 m

After validating the numerical simulation in terms of mean velocity profiles with experimental data, IBM-LES results are used to investigate the overall flow patterns in the stirred tank and evaluate the effect of baffle and impeller on the flow behavior. Fig. 5 shows the predicted two-dimensional velocity contours with velocity vectors, in a central vertical section through the stirred tank in a horizontal section at an axial position (Z = 0.105 m) from the bottom of the stirred tank.

The radial jet originating from the tips of the impeller blades forms secondary swirl rings above and below the impeller. The flow patterns above and away from the impeller are significantly affected and controlled by the baffle. In the upper part of the tank, the baffles break the circular flow caused by the impeller and make the liquid move in more diverse directions. Near the baffles, these vectors are in different directions compared to areas far from the baffles, showing how the flow pattern changes. On the other hand, in the lower parts of the stirred tank, the baffle obstructs the flow and changes the overall flow pattern. The tangential flow in the stirred tank is significantly affected by the two-finger baffle. It is remarkable that the mean flow is not axisymmetric which can be regarded as a consequence of the single two-finger baffle.

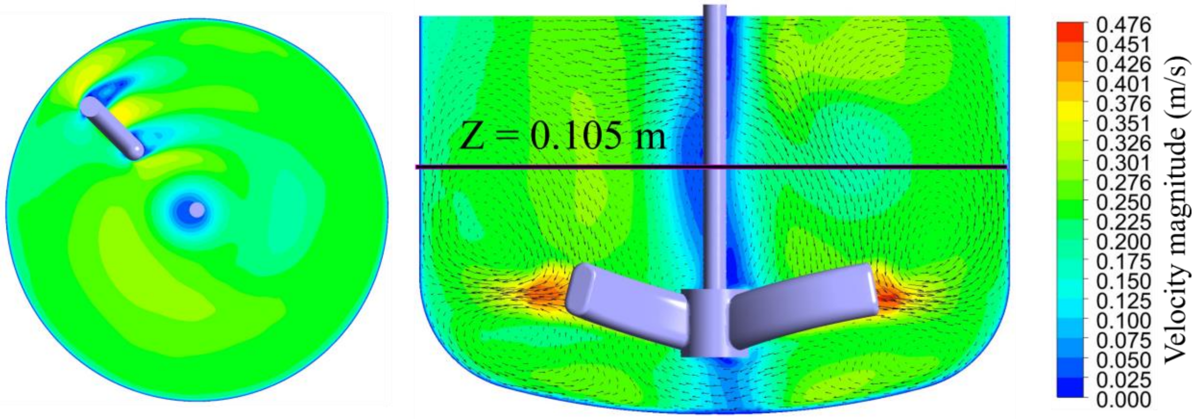

Fig. 5 Flow field contours with mean velocity vectors obtained from IBM-LES

3.2. Kinetic energy

In this section, the statistical convergence of the velocity component variances was initially examined. Convergence for all components was achieved after 11,238 acquisitions. Subsequently, the simulated flow field was validated by comparing the distribution of turbulent kinetic energy. Since the experimental data were obtained using 2D-2C PIV, the numerical results presented are based on only two components of turbulent kinetic energy. Fig. 6 compares the turbulent kinetic energy distribution between IBM-LES and experimental results. In the bottom part of each contour plot, a high amount of turbulent kinetic energy is observed in the region located just above the impeller. Surprisingly, similar amounts of turbulent kinetic energy are also observed in the upper part of the tank, away from the impeller. This point will be re-examined in the last two sections of this work.

As shown in Figure 6, the LES-IBM simulation and experimental data show discrepancies in the kinetic energy distribution. However, evaluating the Taylor micro-scale (2.5–7 mm) confirms that both PIV (pixel size = 0.85 mm) and CFD resolutions (grid resolution = 0.6–2.5 mm) are sufficient to capture turbulence scales. Therefore, these discrepancies can be attributed to the following reasons: (i) boundary condition sensitivity, slight differences in impeller, shaft clearance, wall roughness, or surface imperfections impact turbulence generation, especially in high-shear regions. In this project, only two turbulence components (u′u′ and v′v′) were captured. The captured components are small and highly sensitive to boundary conditions and setup variations; (ii) turbulence's chaotic nature in stirred tanks, with small variations in impeller or baffle wakes causing localized turbulence changes; and (iii) anisotropic turbulence and large-scale coherent structures, which are resolved in LES but smoothed or spatially displaced in PIV due to ensemble-averaging, leading to differences in turbulence features and their locations.

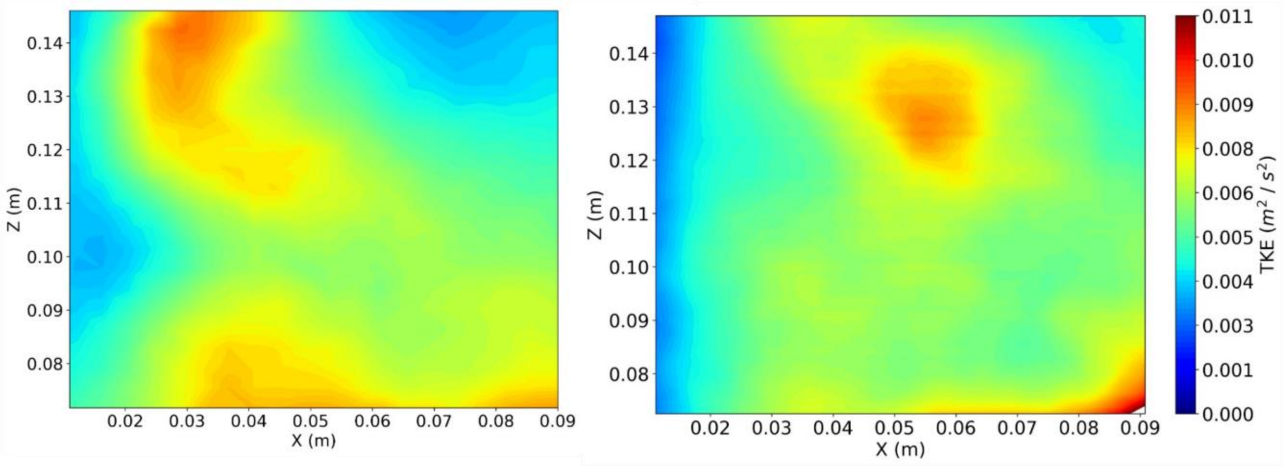

(a) (b)

Fig. 6 Contours of turbulent kinetic energy of the 2D velocity field. (a) PIV data, (b) IBM-LES simulation.

Fig. 7 shows the comparison between the calculated turbulent kinetic energy of the numerical simulations (IBM-LES) and the experimental results for two axial positions of Z = 0.085 m and Z = 0.105 m. There is good agreement between the numerical simulation results and the experimental data in terms of magnitude and shape of turbulent kinetic energy profiles. In addition, the IBM-LES result shows good agreement with the experimental data, especially in the region of high turbulent kinetic energy. This result confirm that the mesh size is fine enough, smaller than the Taylor scale, to capture all kinetic energy scales.

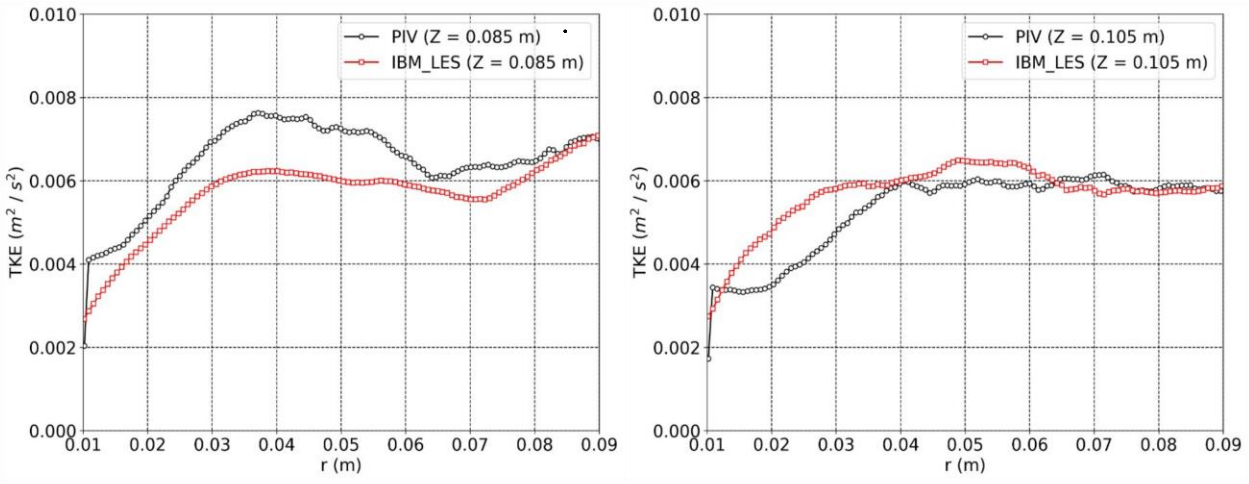

(a) (b)

Fig. 7. Comparison of turbulent kinetic energy profiles at (a) Z = 0.085 m and (b) Z = 0.105 m.

3.3. Turbulence dissipation rate

In LES, part of the energy dissipation is resolved by the mesh while contribution from the smallest scales is quantified through a sub-grid scale model. Assuming a local equilibrium between the production and dissipation of turbulent kinetic energy at the cut-off scale, the sub-grid dissipation rate is here computed using the Smagorinsky constant C_S=0.2. The total energy dissipation rate, combining resolved and sub-grid scales, is depicted in Fig. 8. The results show that the rate of energy dissipation in the tank is very inhomogeneous, its magnitude in the vicinity of the impeller is several times larger than in other areas of the tank. It should be noted that since the mesh size in the current study is about 10 times the Kolmogorov scale, directly resolving all scales of dissipation rate through numerical simulation out of reach. Despite this limitation, the agreement between the predicted turbulent kinetic energy and experimental results suggests a reasonable assumption that the simulations accurately predict the distribution of energy dissipation rates.

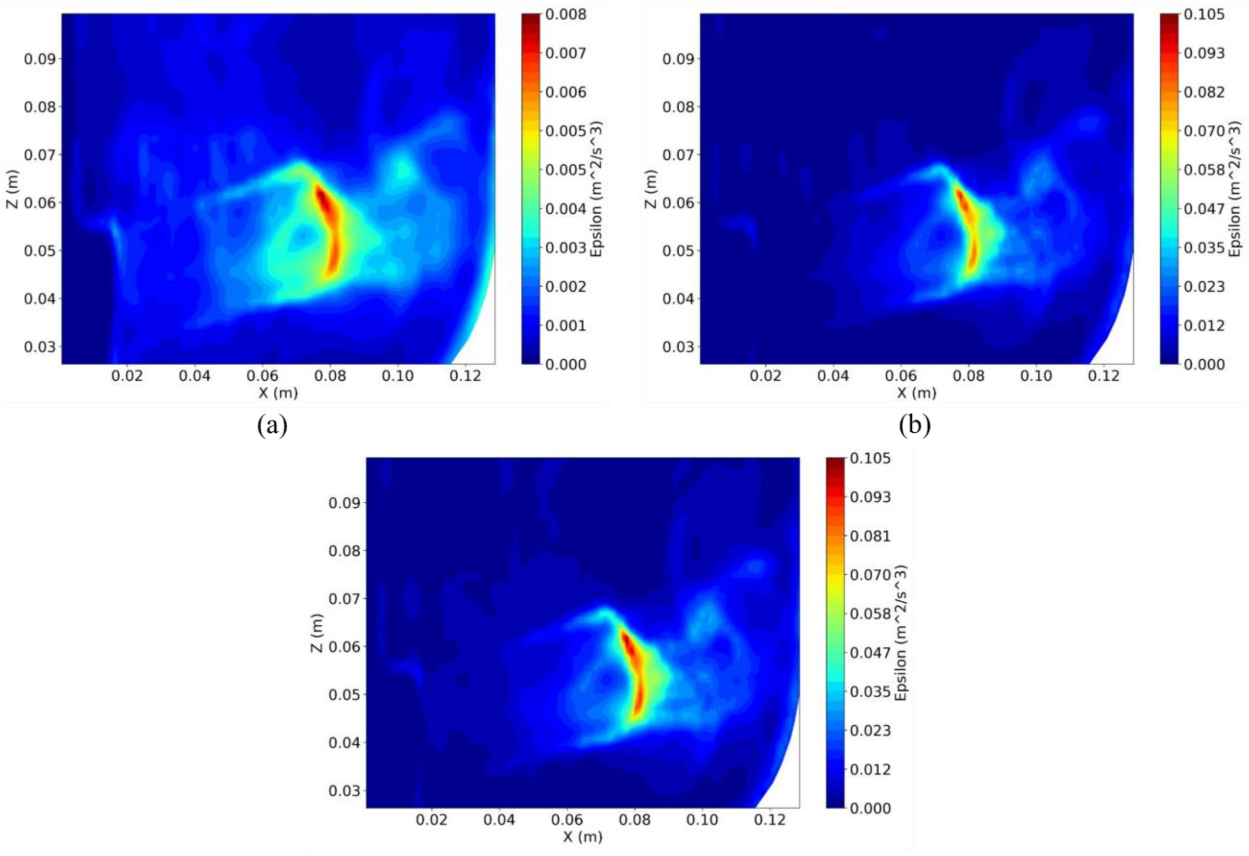

(a) (b)

(c)

Fig. 8. Energy dissipation rate of the IBM-LES: (a) mesh resolved; (b) computed based on the sub-grid model; (c) total energy dissipation rate.

3.4. POD analysis

A POD analysis in now proposed to analyze in more detail the energy content in the impeller zone and in the upper zone where unexpectedly high amount of kinetic energy are found (in the measurement plane). Proper Orthogonal Decomposition (POD) is an effective method for analyzing instantaneous velocity fields, enabling the reconstruction of velocity as a sum of modes ranked according to their contribution to the total kinetic energy. These modes can be obtained from the Fredholm eigenvalue integral equation introduced by Sirovich [40]. The result is an orthonormal basis of eigenfunctions and associated eigenvalues. The instantaneous velocity field can be projected onto each POD eigenfunction. These projections yield POD coefficients, which can be used to reconstruct the instantaneous velocity fields. The POD technique is detailed in the literature [33, 41-43]. In this study, we used the snapshot method on IBM-LES results. More information on our snapshot method can be found in Liné et al. (2013) [41] and Liné (2016) [43]. Since the IBM method performs on a fixed mesh, applying POD to the IBM-LES results is straightforward. Data were collected in four two-dimensional zones located in the same vertical plane, as shown in Fig. 9a. Zone A and B are swept by the impeller, the number of sampling points in each zone is the same. Zone C and D are in the upper part of the tank, here also the number of sampling point is the same in both zones but it is different from that used in zones A and B. The impeller rotates in the clockwise direction so zones A and C are located upstream of the baffle whilst zones B and D are located downstream.

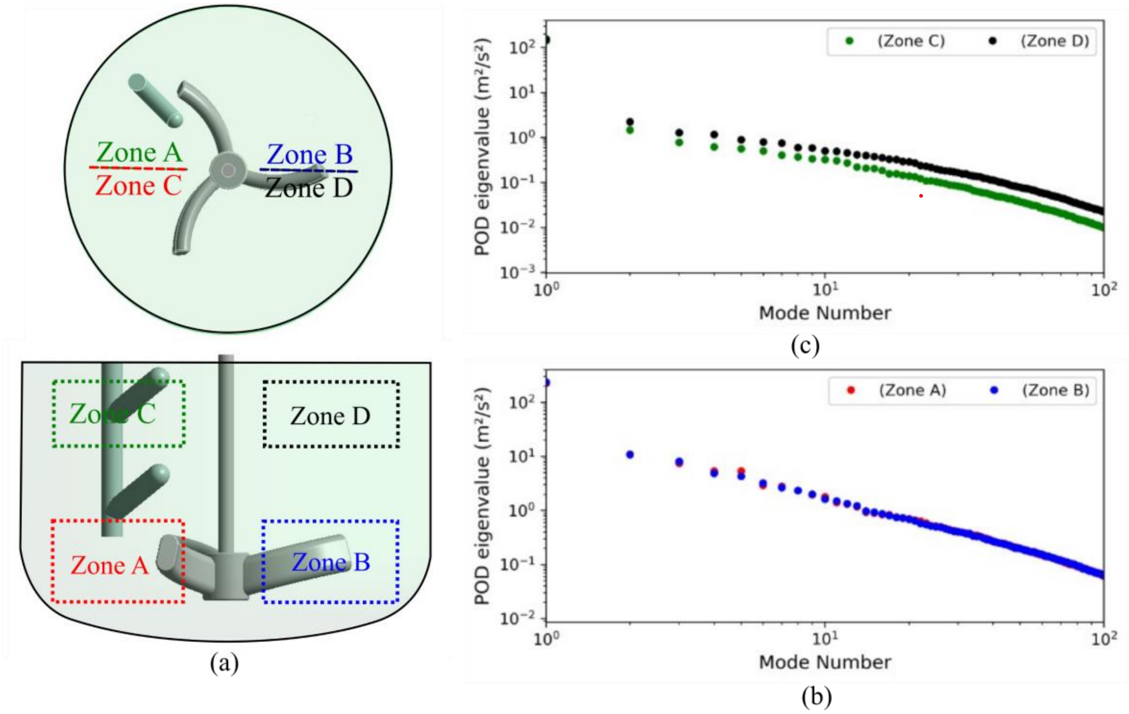

Fig. 9. (a) Zones of interest for POD analysis; (b) Energy spectrum in Zones A and B; (c) Energy spectrum in Zones C and D

Fig. 9b presents the energy spectrum in zone A and B. The total energy content is 293.68 (m^2/s^2) and 304.83 (m^2/s^2) in zone A and B, respectively. There is no significant difference in terms of total energy content between these zones, as the flow is primarily controlled by the impeller. The energy spectra in these two zones are almost similar as shown in Fig. 9b**.** It is however remarkable that mode 4 and mode 5 contains the same amount of energy in the Zone A. This feature is typical of modes associated with organized motion and can thus be related to trailing vortices. In contrast, the energy content of mode 5 in the Zone B is distinctively smaller, which might be the consequence of the interaction of the trailing vortices with the baffle**.**

Fig. 9c presents the energy spectrum in zone C and D. The total energy content expressed as the sum of eigenvalues is 153.32 (m^2/s^2) in Zone C, and goes up to 173.89 (m^2/s^2) in Zone D. The energy content of the first mode is similar in Zones C (143.34 m^2/s^2) and D (153.84 m^2/s^2). This first mode holds for 93.5 % of the total energy content in zone C but only 88.5 % in Zone D. The major difference is visible for higher order modes where the spectrum is shifted upward in Zone D compared to Zone C. Thus, the POD analysis indicates that the energy distribution is different in Zones C and D, the amount of energy related to the mean flow is identical whereas a significantly higher amount of organized and turbulent kinetic energy is found in Zone D, i.e downstream of the baffle in the upper part of the tank, as previously illustrated in Fig. 6.These findings are illustrated by a series of figures provided as supplementary information (**Fig. S8-S10**). The results indicate that in the zone where the impeller controls the flow, the flow kinetic energy is axisymmetric. However, in the regions influenced by the baffle, the fluid exhibits asymmetric behavior, confirming that the baffle affects the flow.

3.5. Trailing vortex identification according to Jeong and Hussain technique

In order to confirm the hypothesis that the baffle is responsible for unfamiliar spatial distribution of kinetic energy in such a tank, the method of Jeong and Hussain was used to visualize the presence of coherent structures such as trailing vortices formed behind the impeller blades [44]. According to this method, based on the strain rate tensor and rotation rate tensor, the core of the trailing vortex is defined by a region where the second eigenvalue λ_2 of the $S^2+\Omega^2$ tensor is negative. S and Ω are the symmetric and the anti-symmetric parts of the velocity gradient tensor respectively

$$S_{ij} = \frac{1}{2}\left(\frac{\partial u_i}{\partial x_j} + \frac{\partial u_j}{\partial x_i}\right) \tag{18}$$

$$\Omega_{ij} = \frac{1}{2}\left(\frac{\partial u_i}{\partial x_j} - \frac{\partial u_j}{\partial x_i}\right) \tag{19}$$

Using nine components of these velocity gradient tensor stored in the database, the symmetric (S) and antisymmetric (Ω) parts of the velocity gradient tensor are estimated. These two tensors were evaluated in each k-plane to determine the shape of trailing vortices every 1.2˚.

The iso-surface depicted in Fig. 10 illustrates the development of a trailing vortex behind both the impeller blades and baffle fingers at a rotational speed of 100 rpm, with the impeller rotating in a clockwise direction. In Fig. 10a, two distinct trailing vortices are observed in the wake of the impeller blades. Their aspect is typical of trailing vortices produced by radial impeller [45]. These vortices contribute to both the radial jet flow and intense mixing in this zone. Note that the bottom tip of the baffle interacts with these trailing vortices, whilst other trailing vortices have similar extent and size. Fig. 10b illustrates the presence of coherent structures attached to the baffle fingers and caused by the interaction of the orthoradial flow with the cylindrical obstacles. These coherent structures develop over about 100 degrees, contributing to the dissymmetry of the mean flow field visible in Fig. 5. Along with the analysis of the energy content of the flow brought by the POD visible in Fig. 10c, it can be concluded that this extra amount of turbulent kinetic energy comes from the coherent structures which develop in the wake of the baffle.

Based on the information presented above, the presence of a two-finger baffle alters the flow field structure in the stirred tank by influencing the spatial energy distribution and forming trailing vortices. In terms of energy transfer mechanisms, the two-finger baffle creates localized regions of flow that act as sources of instabilities in the flow structure. As shown in Fig. 10, these instabilities promote the production of smaller-scale vortices, thereby enhancing the cascade of kinetic energy. Additionally, the interaction between the flow generated by the impeller and that generated by the two-finger baffle further intensifies this process, resulting in high kinetic energy downstream of the baffle. In terms of vortices formation, in this stirred tank, two types of trailing vortices are formed. The primary trailing vortices result from tip leakage flow at the impeller blade tip and shear stresses along the blade edges. The secondary vortices develop at the edges of the two-finger baffle due to flow separation. Near the region where the baffle and impeller are close, the impeller-induced flow interacts with the baffle. This interaction causes flow blockage and deflection around the baffle fingers, leading to vortex stretching and partial fragmentation. So, the interaction between these two vortices creates complex vortex dynamics in the tank, disrupting the coherence of the wake vortices. This results in smaller, less coherent structures as they propagate downstream. This mechanism aligns with the findings shown in Fig. 10, based on Jeong and Hussain's vortex identification method.

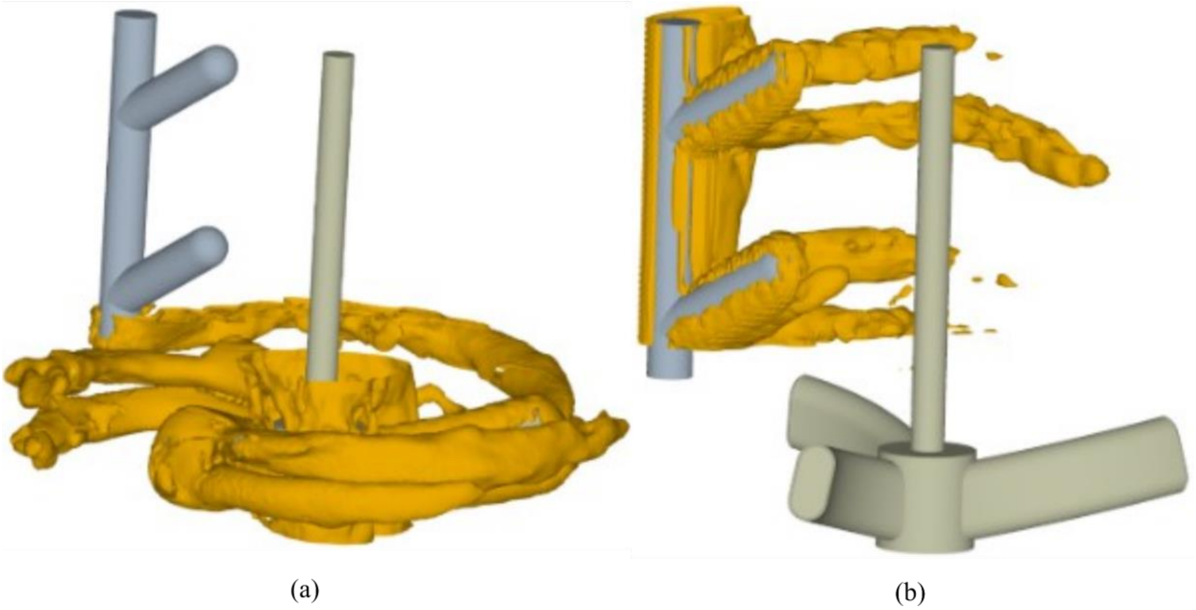

Fig. 10. Visualization of the trailing vortices in the simulation volume based on Jeong and Hussain's technique: (a) behind the impeller; (b) behind the baffle

Altogether, these multiple interactions lead to a complex flow structure where a strong turbulence anisotropy is at stake. In that situation, IBM-LES is a valuable modeling choice to describe the dynamics of this flow field.

5. Summary and conclusions

In the present work, IBM-LES simulation was performed to analyze the hydrodynamic behavior in a stirred tank equipped with a retreat blade impeller and a two-finger baffle. The results of the numerical simulations were evaluated using detailed PIV data. The first goal of this paper was to evaluate the possibility of using the IBM approach in predicting the fluid behavior of a stirred tank with a complex geometrical configuration under high Reynolds number operating conditions. Upon comparing the numerical predictions of IBM-LES with PIV data, a commendable agreement was identified between the simulation and experimental results in terms of mean velocities and turbulent kinetic energy. In addition, the mesh generation process for a stirred tank with complex geometric configurations is significantly simpler with IBM-LES, especially here where the distance between the tip of the blade and the baffle is very small.

The second objective of the paper was to evaluate the effect of the retreating blade impeller and a two-finger baffle on the hydrodynamic characteristics of the stirred tank using IBM-LES results. In contrast to other numerical strategies involving a moving mesh, the IBM-LES technique allows to perform a POD treatment of numerical results readily, in a baffled tank, despite the presence a rotating impeller, because the location of mesh nodes is time-independent. The POD analysis of the IBM-LES results confirmed that the high energy level found in the upper part of the tank is related to the energy transfer from the coherent structures created downstream the two-finger baffle. Finally, in addition, this study identifies and characterizes trailing vortices created behind the impeller blade and two-finger baffle. Trailing vortices were identified using Jeong and Hussain's technique, which relies on an objective definition of vortical structures. The findings indicate a significant influence of the baffle on the flow patterns above and away from the impeller. In particular, the two-finger baffle significantly affects the tangential flow in the stirred tank. The outcomes of trailing vortices identification indicate the formation of two separate trailing vortices behind both the impeller blades and the baffle fingers.

Acknowledgments: The authors thank the Agence Nationale de la Recherche (ANR) in France which founded this research, project ANR-20-CE07–0025-01.

References

[1] A.W. Nienow, M.F. EDWARDS, N. Harnby, Mixing in the process industries, Butterworth-Heinemann1997.

[2] P.J. Cullen, Food mixing: Principles and applications, John Wiley & Sons2009.

[3] E.L. Paul, V.A. Atiemo-Obeng, S.M. Kresta, Handbook of industrial mixing, Wiley Online Library2004.

[4] F. Alberini, L. Liu, E.H. Stitt, M.J.H. Simmons, Comparison between 3-D-PTV and 2-D-PIV for determination of hydrodynamics of complex fluids in a stirred vessel, Chemical Engineering Science 171 (2017) 189-203. https://doi.org/https://doi.org/10.1016/j.ces.2017.05.034.

[5] R. Escudié, A. Liné, Experimental analysis of hydrodynamics in a radially agitated tank, AIChE Journal 49(3) (2003) 585-603.

[6] A. Delafosse, A. Line, J. Morchain, P. Guiraud, LES and URANS simulations of hydrodynamics in mixing tank: comparison to PIV experiments, Chemical Engineering Research and Design 86(12) (2008) 1322-1330.

[7] G.L. Lane, Improving the accuracy of CFD predictions of turbulence in a tank stirred by a hydrofoil impeller, Chemical Engineering Science 169 (2017) 188-211.

[8] M. Wu, N. Jurtz, A. Walle, M. Kraume, Evaluation and application of efficient CFD-based methods for the multi-objective optimization of stirred tanks, Chemical Engineering Science 263 (2022) 118109.

[9] M. Campolo, A. Paglianti, A. Soldati, Fluid dynamic efficiency and scale-up of a retreated blade impeller CSTR, Industrial & engineering chemistry research 41(2) (2002) 164-172.

[10] J. Luo, Prediction of impeller induced flows in mixing vessels using multiple frames of reference, I. Chem. E. Symposium Series, 1994, pp. 549-556.

[11] C. Harris, D. Roekaerts, F. Rosendal, F. Buitendijk, P. Daskopoulos, A. Vreenegoor, H. Wang, Computational fluid dynamics for chemical reactor engineering, Chemical Engineering Science 51(10) (1996) 1569-1594.

[12] J. Murphy, CFD simulation of flows in stirred tank reactors using a sliding mesh technique, Instn. Chem. Engng. Symp. Ser., 1994, pp. 341-348.

[13] S.L. Yeoh, G. Papadakis, K.C. Lee, M. Yianneskis, Large eddy simulation of turbulent flow in a Rushton impeller stirred reactor with sliding-deforming mesh methodology, Chemical Engineering & Technology: Industrial Chemistry-Plant Equipment-Process Engineering-Biotechnology 27(3) (2004) 257-263.

[14] C.S. Peskin, Flow patterns around heart valves: a numerical method, Journal of computational physics 10(2) (1972) 252-271.

[15] G. Montante, A. Bakker, A. Paglianti, F. Magelli, Effect of the shaft eccentricity on the hydrodynamics of unbaffled stirred tanks, Chemical Engineering Science 61(9) (2006) 2807-2814. https://doi.org/https://doi.org/10.1016/j.ces.2005.09.021.

[16] A. Tamburini, A. Brucato, M. Ciofalo, G. Gagliano, G. Micale, F. Scargiali, CFD simulations of early- to fully-turbulent conditions in unbaffled and baffled vessels stirred by a Rushton turbine, Chemical Engineering Research and Design 171 (2021) 36-47. https://doi.org/https://doi.org/10.1016/j.cherd.2021.04.021.

[17] A. Posa, A. Lippolis, R. Verzicco, E. Balaras, Large-eddy simulations in mixed-flow pumps using an immersed-boundary method, Computers & Fluids 47(1) (2011) 33-43.

[18] H. Luo, R. Mittal, X. Zheng, S.A. Bielamowicz, R.J. Walsh, J.K. Hahn, An immersed-boundary method for flow–structure interaction in biological systems with application to phonation, Journal of computational physics 227(22) (2008) 9303-9332.

[19] D. Kim, H. Choi, Immersed boundary method for flow around an arbitrarily moving body, Journal of Computational Physics 212(2) (2006) 662-680.

[20] M. Uhlmann, An immersed boundary method with direct forcing for the simulation of particulate flows, Journal of computational physics 209(2) (2005) 448-476.

[21] W.-P. Breugem, A second-order accurate immersed boundary method for fully resolved simulations of particle-laden flows, Journal of Computational Physics 231(13) (2012) 4469-4498.

[22] R. Verzicco, M. Fatica, G. Iaccarino, P. Orlandi, Flow in an impeller-stirred tank using an immersed-boundary method, AIChE journal 50(6) (2004) 1109-1118.

[23] M. Tyagi, S. Roy, A.D. Harvey Iii, S. Acharya, Simulation of laminar and turbulent impeller stirred tanks using immersed boundary method and large eddy simulation technique in multi-block curvilinear geometries, Chemical Engineering Science 62(5) (2007) 1351-1363.

[24] S. Roy, S. Acharya, M.D. Cloeter, Flow structure and the effect of macro-instabilities in a pitched-blade stirred tank, Chemical Engineering Science 65(10) (2010) 3009-3024.

[25] S. Roy, S. Acharya, Scalar mixing in a turbulent stirred tank with pitched blade turbine: Role of impeller speed perturbation, Chemical Engineering Research and Design 90(7) (2012) 884-898.

[26] B. Blais, M. Lassaigne, C. Goniva, L. Fradette, F. Bertrand, A semi-implicit immersed boundary method and its application to viscous mixing, Computers & Chemical Engineering 85 (2016) 136-146.

[27] J. Joachim, C.-A. Daunais, V. Bibeau, L. Heltai, B. Blais, A parallel and adaptative Nitsche immersed boundary method to simulate viscous mixing, Journal of Computational Physics 488 (2023) 112189.

[28] M. Campolo, A. Soldati, Appraisal of fluid dynamic efficiency of retreated-blade and turbofoil impellers in industrial-size CSTRs, Industrial & engineering chemistry research 41(5) (2002) 1370-1377.

[29] M. Li, G. White, D. Wilkinson, K.J. Roberts, Scale up study of retreat curve impeller stirred tanks using LDA measurements and CFD simulation, Chemical Engineering Journal 108(1-2) (2005) 81-90.

[30] C. Rielly, M. Habib, J.-P. Sherlock, Flow and mixing characteristics of a retreat curve impeller in a conical-based vessel, Chemical Engineering Research and Design 85(7) (2007) 953-962.

[31] C. Sirasitthichoke, P.M. Armenante, Power dissipation and power number correlations for a retreat-blade impeller under different baffling conditions, Industrial & Engineering Chemistry Research 56(36) (2017) 10123-10133.

[32] C. Sirasitthichoke, S. Salloum, P.M. Armenante, Power number and hydrodynamic characterization of a stirred vessel equipped with a Retreat-Blade Impeller and different types of pharmaceutical single baffles, Chemical Engineering Science 257 (2022) 117725. https://doi.org/https://doi.org/10.1016/j.ces.2022.117725.

[33] C. Mayorga, J. Morchain, A. Liné, Reconstruction of the 3D hydrodynamics in a baffled stirred tank using proper orthogonal decomposition, Chemical Engineering Science 248 (2022) 117220.

[34] E.A. Fadlun, R. Verzicco, P. Orlandi, J. Mohd-Yusof, Combined immersed-boundary finite-difference methods for three-dimensional complex flow simulations, Journal of computational physics 161(1) (2000) 35-60.

[35] J. Smagorinsky, General circulation experiments with the primitive equations: I. The basic experiment, Monthly weather review 91(3) (1963) 99-164.

[36] N.D. Katopodes, Chapter 8 - Turbulent Flow, in: N.D. Katopodes (Ed.), Free-Surface Flow, Butterworth-Heinemann2019, pp. 566-650. https://doi.org/https://doi.org/10.1016/B978-0-12-815489-2.00008-3.

[37] B. Galperin, S.A. Orszag, Large eddy simulation of complex engineering and geophysical flows, (1993).

[38] P. Sagaut, Introduction à la simulation des grandes échelles pour les écoulements de fluide incompressible, Springer Science & Business Media1998.

[39] P. Saarenrinne, M. Piirto, H. Eloranta, Experiences of turbulence measurement with PIV, Measurement Science and Technology 12(11) (2001) 1904.

[40] L. Sirovich, Turbulence and the dynamics of coherent structures. I. Coherent structures, Quarterly of applied mathematics 45(3) (1987) 561-571.

[41] A. Liné, J.-C. Gabelle, J. Morchain, D. Anne-Archard, F. Augier, On POD analysis of PIV measurements applied to mixing in a stirred vessel with a shear thinning fluid, Chemical Engineering Research and Design 91(11) (2013) 2073-2083.

[42] J. Moreau, A. Liné, Proper orthogonal decomposition for the study of hydrodynamics in a mixing tank, AIChE journal 52(7) (2006) 2651-2655.

[43] A. Liné, Eigenvalue spectrum versus energy density spectrum in a mixing tank, Chemical Engineering Research and Design 108 (2016) 13-22.

[44] J. Jeong, F. Hussain, On the identification of a vortex, Journal of fluid mechanics 285 (1995) 69-94.

[45] A. Delafosse, J. Morchain, P. Guiraud, A. Liné, Trailing vortices generated by a Rushton turbine: Assessment of URANS and large Eddy simulations, Chemical Engineering Research and Design 87(4) (2009) 401-411.